Physical Biology

OFFICIAL JOURNAL OF
Sociedad de Biofísicos Latino Americanos

ACCEPTED MANUSCRIPT

Morphology and dynamics of tumor cell colonies propagating in epidermal growth factor supplemented media

To cite this article before publication: Nicolás Eduardo Muzzio *et al* 2018 *Phys. Biol.* in press https://doi.org/10.1088/1478-3975/aabc2f

Morphology and dynamics of tumor cell colonies propagating in epidermal growth factor supplemented media

N E Muzzio[1], M Carballido[2], M A Pasquale[1], P H González[3], O Azzaroni[1] and A J Arvia[1]

[1] Instituto de Investigaciones Fisicoquímicas Teóricas y Aplicadas (INIFTA), Universidad Nacional de La Plata (UNLP), CONICET, Sucursal 4, Casilla de Correo 16, 1900, La Plata, Argentina

[2] Facultad de Ciencias Exactas, UNLP, Calle 47 y 116, 1900, La Plata, Bs. As., Argentina

[3] Cátedra de Patología, Facultad de Ciencias Médicas, UNLP, CICBA, Calle 60 y 120, 1900, La Plata, Bs. As., Argentina

Abstract. The epidermal growth factor (EGF) plays a key role in physiological and pathological processes. This work reports on the influence of EGF concentration (c_{EGF}) on the modulation of individual cell phenotype and cell colony kinetics with the aim of perturbing the colony front roughness fluctuations. For this purpose, HeLa cell colonies that remain confluent along the whole expansion process with initial quasi-radial geometry and different initial cell populations, as well as colonies with initial quasi-linear geometry and large cell population, are employed. Cell size and morphology as well as its adhesive characteristics depend on c_{EGF}. Quasi-radial colonies (QRC) expansion kinetics in EGF-containing medium exhibits a complex behavior. Namely, at the first stages of growth, the average QRC radius evolution can be described by a $t^{1/2}$ diffusion term coupled with exponential growth kinetics up to a critical time, and afterwards a growth regime approaching constant velocity. The extension of each regime depends on c_{EGF} and colony history. In the presence of EGF, the initial expansion of quasi-linear colonies (QLCs) also exhibits morphological changes at both the cell and the colony levels. In these cases, the cell density at the colony border region becomes smaller than in the absence of EGF and consequently, the extension of the effective rim where cell duplication and motility contribute to the colony expansion increases. QLC front displacement velocity increases with c_{EGF} up to a maximum value in the 2 – 10 ng ml^{-1} range. Individual cell velocity is increased by EGF, and an enhancement in both the persistence and the ballistic characteristics of cell trajectories can be distinguished. For an intermediate $c_{EGF,}$ collective cell displacements contribute to the roughening of the colony contours. This global dynamics becomes compatible with the standard Kardar-Parisi-Zhang growth model, although a faster colony roughness saturation in EGF-containing medium than in the control medium is observed.

Keywords: epidermal growth factor, HeLa cell, colony kinetics, dynamic scaling, cell transport mechanism.

PACS numbers: 87.17.Ee,87.17.Jj,87.18.Gh,87.18.Hf,87.16.dr,89.75.Da

1. Introduction

The stimulation of cell growth and motility plays a key role in many physiological and pathological processes such as morphogenesis, wound healing and tumor propagation, the coordinated displacement of cells being of relevance [1-4]. The epidermal growth factor (EGF) stimulates a large number of cell phenotypes involved in those biological processes [5-8]. EGF binds a plasma membrane receptor tyrosine kinase [9] and enhances cell proliferation and migration. However, the effect of EGF depends on the cell type, either normal or neoplastic, triggering important mechanisms differently according to the cell type [10]. It has also been reported from scratch assays of intestinal epithelial cell data [11] that EGF-induced cell motility patterns render a repopulated zone with a larger number of voids in comparison with control experiments involving other stimulating species. In fact, a milieu of growth factors is secreted immediately after wounding, and the relation of each one to cell motility behavior is of relevance for interpreting the underlying mechanism of the repopulation process [12].

On the other hand, the EGF-induced cell scattering in vitro model for studying epithelial-mesenchymal transition (EMT) recapitulates many events that occur during EMT, including the dissociation of multicellular structure and increased cell motility [13]. More recently, it has been reported that individual cell motility is affected by either soluble [14, 15] or immobilized EGF [16, 17], increasing the collective monolayer displacement, although in the case of immobilized EGF, there is a significant increase in the cell displacement persistence. Cell movements are often guided by chemical cues, and the chemoattractant molecules bind to surface receptors on the membrane and activate intracellular signals. In general, cells move in interacting groups rather than in an isolated manner [18, 19]. Although the mechanism of individual cell motion induced by chemoattractants has been rather extensively studied, the displacement characteristics of cell groups determining their directionality is much less understood [20]. It has been reported that cell-cell communication enhances the sensitivity of cell ensemble to chemoattractant gradients [21].

Recently, it has been reported that the collective displacement undergoes by intermittent bursts of certain extensions of the cell monolayer, similar to those observed in the flow of liquids in porous media. This behavior is independent of the type of cell and the nature of the substrate [22]. Other universal behaviors, found either in inanimate or living systems, have also been reported [23-25]. Constituents of living systems interact

in a cooperative manner and determine the global system behavior. Then, for instance, the properties of the resulting interface can be described by its fractality by applying different statistical techniques such as the dynamic scaling analysis to access the spatial and scale dependence of colony interface fluctuations. In this approach, the two-dimensional (2D) cell colony front dynamics can be interpreted based upon a set of dynamic scaling exponents (α, β, z, the roughness, the growth and the dynamic exponents, respectively) derived from the dynamic scaling analysis of colony front profiles, and by comparing these results to those expected from different statistical growth models [26-27]. Experimental data from non-Euclidean 2D spreading biological interfaces were interpreted, at least within certain ranges of colony front length and age, in terms of the standard Kardar, Parisi and Zhang (KPZ) continuous equation [28-30]. The evolution of other systems in nature has been recently analyzed in terms of the KPZ model, such as wall roughness of two-dimensional Pt/Co/Pt thin films [31], the growth of semiconductor thin films [32], among others. A characteristic feature of the standard KPZ equation is the nonlinear term that in the case of cell colonies can be related to the anisotropic cell displacements towards free space at the colony border [26, 33].

A large number of studies aiming to elucidate several biochemical mechanisms in which either EGF or its receptors play a key role have been reported [34]. In contrast, papers dealing with the effect of EGF on the global cell colony dynamics [35] of different initial geometry and cell population are rather scarce. The cell colony front velocity data, measured from the average colony radius ($<R>$) of initial quasi-radial colonies (QRCs), or the linear average displacement distances from a reference position, in the case of quasi-linear colonies (QLCs), allow us to distinguish the effect of some cooperative behavior modulated by EGF concentration (c_{EGF}) on the global dynamics. Several works have demonstrated the increase in cell motility for a certain range of c_{EGF} [36, 37] and the dispersion effect on cell colonies [13]. In the same vein, the hepatocyte growth factor (HGF) has been employed to perturb the colony border expansion pattern by inducing cell dispersion [38]. Considering these facts, it is interesting to hypothesize that EGF would change some characteristics of the roughness fluctuation process due to its mitogenic and motogenic effect described in the frame of the KPZ equation and integrating phenomena at the cellular and colony scale.

In the present work, colonies that remain confluent during the follow-up are susceptible of being characterized by their displacement distance and their roughness evolution.

Results show that within certain range of c_{EGF}, the colony front dynamics depends on both the initial cell population and the colony cell density. Accordingly, the presence of EGF contributes to modifying the local cell density heterogeneity by local changes in the size and shape of the cells, affecting cell motility characteristics. The latter effect involves a first cell adhesion step followed by its expansion and propagation, i.e. all these processes depend on the cytoskeleton reorganization. The presence of EGF modifies the amount and size of focal contacts. Furthermore, in the presence of EGF within a certain concentration range, cell displacements become more persistent and ballistic and with a greater contribution of lateral components than in the plain medium, influencing the global dynamics of large population colonies characterized by the front roughness evolution. Thus, dynamic data from colonies growing in EGF-containing medium are consistent with the predictions of the standard Kardar-Parisi-Zhang equation, although the roughness saturation is approached earlier than for cell colonies in the control medium.

2. Experimental

2.1. Colony preparation procedures

HeLa cells, passage 44-60, were employed. Cell colonies were cultured in polystyrene Petri dishes 3.6 cm in diameter (Greiner Bio One), employing Roswell Park Memorial Institute (RPMI) medium supplemented with 10 % fetal bovine serum (FBS), 2 g l^{-1} bicarbonate, and 100 μM ml^{-1} streptomycin. Epidermal growth factor in the 0 – 50 ng ml^{-1} concentration range was added to the culture medium. The cultures were incubated at 37 °C in a sterilized atmosphere with 5% carbon dioxide and 97% humidity. As required, half of the medium was changed every 2 days to maintain its composition practically constant. Cell viability was achieved by Trypan blue vital staining. The culture medium, antibiotic and EGF were acquired from Life Technologies.

Each QRC was grown by seeding 2 ml of supplemented medium containing 1000–2000 cells into Petri dishes, where they adhere to the dish bottom. After growing for 4–5 days, the culture consisted of colonies with a different number of cells (N_0) at the time t_0 at which colony growth data collection started.

QLCs were prepared as described elsewhere [30] utilizing a sterilized Teflon® tape 2.2 cm wide and 100 μm thick to cover the central region of a Petri dish bottom. Subsequently, 2 ml of a suspension of 20,000 cells ml^{-1} in supplemented medium was

seeded. Cell duplication produced a number of colonies spreading on the remaining Petri dish bottom free surface. Then, about 2 days later, when a confluent cell monolayer was formed, the Teflon tape was removed. In these runs, in contrast to QRC colonies, to avoid the influence of cell confinement, spreading data were collected about 12 h after removing the Teflon tape.

2.2. Colony growth pattern microimaging

Colony growth patterns were imaged using a Nikon DS-Fi digital camera coupled to a Nikon TS100 phase-contrast inverted microscope with a CFI flat field ADL 10X objective. The image resolution was 1 μm = 2.1 pixel. The colony growth time (t) was counted from t_0, the time from which data were collected, except for those experiments in which another reference time was selected, as is indicated further on.

In situ cell colony digital images were obtained for 2–3 days by a time-lapse system at intervals in the range $5 \leq \Delta t' \leq 45$ min. For this purpose, QLCs were placed inside an isolated chamber fixed to the microscope platform to maintain the cultures at 37 ºC and 97% humidity. For preserving the pH, before placing each Petri dish in the chamber, the culture medium was changed to RPMI CO_2-Independent Medium (Gibco, Invitrogen Corp.). Occasionally, the culture medium was replaced by fresh RPMI bicarbonate supplemented medium under a 5% CO_2-air atmosphere. Both media contained L-glutamine and streptomycin.

2.3. *Cell immunostaining*

Fluorescent staining of vinculin, actin and cell nucleus was carried out to study cell adhesion. The staining was done following the protocol described in the Actin Cytoskeleton and Focal Adhesion Staining Kit user manual. Cultured cells were washed with PBS containing 0.05% Tween-20 and fixed with 4% paraformaldehyde. Then, glass cover slips were washed, and cells were permeabilized with 0.1% Triton X-100 in PBS for 5 min. After washing, a blocking solution, 1% BSA in PBS, was applied for 30 min. Then, the antivinculin antibody diluted in the blocking solution was added and incubated for 1 h, followed by washing. The anti-mouse IgG-FITC conjugated antibody diluted in PBS was added to the samples and incubated for 1 h. TRITC-conjugated phalloidin was incubated simultaneously with the second antibody for double labelling. After washing, nucleus counterstaining was performed by incubating cells with DAPI for 5 min. These samples were washed and mounted on a slide by using antifade

mounting solution. Stained cells were observed by an Epi-fluorescence IX 50 Olympus microscope. The number and area of focal contacts were evaluated employing ImageJ software and following the procedure proposed in [39].

2.4. Colony data processing

Colony fronts were manually traced using a Wacom graphic table; the trace error from zoomed images of colony growth patterns resulted in the order of 1 pixel. For data processing, an in-lab developed program was utilized. For QLC at time t, the instantaneous vertical advancing distance, the height of the ith point at the colony front ($h_i(t)$, i = 1, 2, …n), and the mean colony distance $\langle h \rangle = \sum_i h_i(t)/n$ were evaluated. Similarly, for QRC the colony center of mass (CM), the instantaneous distance ($R_i(t)$) from CM to the ith point at the front, and the mean colony radius $\langle R \rangle = \sum_i R_i(t)/n$ were determined.

For QLC with front of size L, the instantaneous global roughness of the expanding front was determined as the standard deviation of the height fluctuations

$$w(L,t) = \left\{ \frac{1}{N} \sum \left[h_i - \langle h \rangle \right]^2 \right\}^{1/2} \quad \textbf{(1)}$$

In this equation, h_i is the maximum instantaneous height at each i point of the colony border. The local roughness, $w(l,t)$, of each colony front was determined in the range $100 \leq l \leq L$ μm.

2.5. Individual cell trajectories

Trajectories of selected cells were measured from the instantaneous 2D coordinates ($\mathbf{P}_j = \mathbf{p}(t_i) = x_j(t_i), y_j(t_i), t_i = 1, 2, \ldots n$) by manually tracking time-lapse movie frames employing Image-Pro Plus 6.0 software, Media Cybernetics Inc.

Coordinate evaluations were referred to either the cell nucleus or the centroid position of each cell contour drawn. From an average of 10 trajectories followed for about 24 h, the difference between both procedures was about 10%. From coordinate data, the mean cell velocity $\langle V_i \rangle$ was evaluated from the equation

$$\langle V_i \rangle = \frac{\mathbf{p}_j(t_{i+1}) - \mathbf{p}_j(t_i)}{\Delta t'} \quad \textbf{(2)}$$

Celerity, velocity components parallel (V_{par}) and perpendicular (V_{per}) to the colony front were evaluated within the interval $15 \leq \Delta t' \leq 45$ min. Considering the small error in the determination of each cell nucleus location, the same average velocity was obtained irrespective of the values of $\Delta t'$.

The mean square displacement was evaluated from the following equation

$$msd = \left\langle \left((x_i(t_0 + \Delta t) - x_i(t_0))^2 \right) + \left((y_i(t_0 + \Delta t) - y_i(t_0))^2 \right) \right\rangle \quad \textbf{(3)}$$

where t_0 is the starting time of the recording interval (Δt). Average data from all values of t_0 and all cell trajectories were derived following reference [40].

The *msd* dependence on Δt approached the power law

$$<msd(\Delta t)> \propto (\Delta t)^b \quad \textbf{(4)}$$

the constant *b* being 1 for a cell with random walk displacement, and 2 for a cell with ballistic displacement [41].

The persistence was calculated as the time needed for the cell to change its displacement direction by 45 degrees.

Cell motility was also studied by particle image velocimetry [42] using PIVlab 1.35 software [43] for MATLAB (The MathWorks, Natick, MA). Image sequences recorded for 500 min with $\Delta t'$ in the 15 – 45 min range were filtered and analyzed with an interrogation window of 82 x 82 pixels with 50% overlap.

3. Results

3.1. Quasi-radial colonies

3.1.1. Morphology. QRCs were grown in a culture medium supplemented with c_{EGF} = 0, 0.08, 0.4, 2 and 10 ng ml^{-1}, and followed by optical microscopy. The follow-up covered the first stages of the colony growth up to 10,000 min and only colonies that remain confluent were considered (figure 1). QRCs with N_0 < 100 cells, cell density < 0.0007 cells μm^{-2}, in culture media with c_{EGF} > 0.4 ng ml^{-1} rendered disaggregated colonies that were not susceptible to be quantitatively followed up by their average radius (See supplementary data, SI).

Tumor cell colonies in EGF supplemented medium

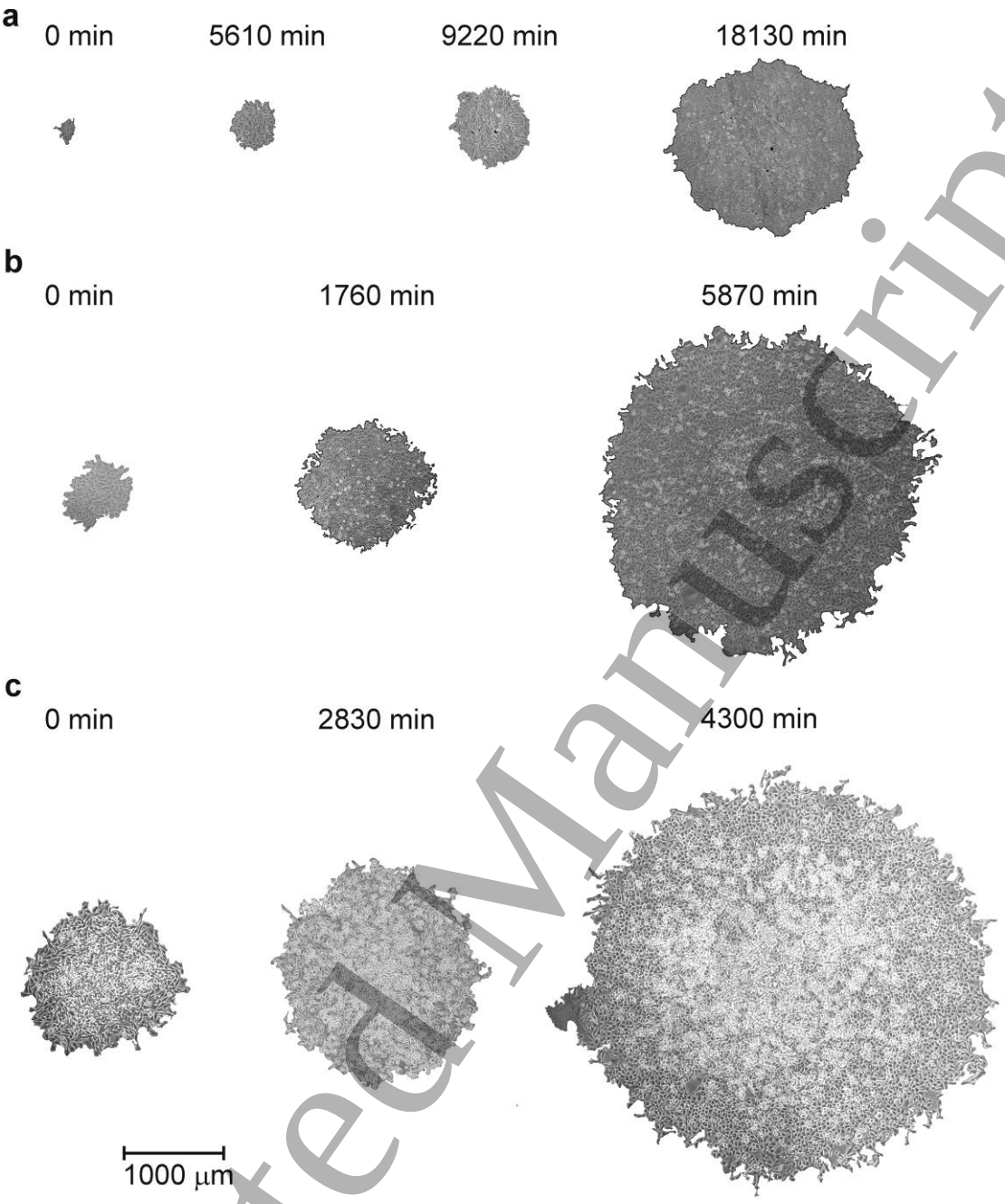

Figure 1. Evolution of cell colony growth pattern sequences in culture media supplemented with c_{EGF}: (a) 0; (b) 0.4; and (c) 10 ng ml^{-1}.

In the absence of EGF (figures 1 and S1), at the first stages of growth the average cell size remained almost constant, but the local cell density increased at the colony bulk and diminished at the colony border region. Finally, at longer stages of growth, the incipient appearance of a 3D phase of cells, cell aggregates above the monolayer, at inner colony regions was observed. In previous works we described the cell 3D phase

formation more completely, and showed stained colonies to allow a clearer visualization of cell aggregates [29, 33].

On the other hand, colonies growing in the c_{EGF} = 0.4 ng ml^{-1} medium for t up to about 2000 min (figure 1b) exhibited a cell density decrease along the whole colony, but later, the cell density increased and tended to remain rather uniform over the entire colony.

For c_{EGF} = 10 ng ml^{-1}, a typical cell colony with $N_0 \approx 1300$ cells and an initial cell density close to 0.00272 cells μm^{-2} (figure 1c) exhibited a first slight colony density decrease at border regions, then a large cell density increase at inner colony regions, and at longer time the formation of a homogeneously distributed 3D cell phase made of quasi-spherical cells of 10 μm diameter or thereabouts. It is worth noting that the cell morphology evolution and the dynamics of 3D phase formation differ considerably from that observed above either in the absence of EGF or at relatively low c_{EGF}. In the former, the 3D phase is made up of a large number of rounded disaggregated cells or small groups of them, whereas for the latter, the 3D phase consists of highly dense cell aggregates. As has been described previously [29], at inner regions of the colony with appropriate cell density, there would be a space restriction for either cells at the monolayer or new born cells to interact with the substrate, tending to locate on upper planes above the monolayer and forming rather compact aggregated or disaggregated cells for c_{EGF} = 0 or in the presence of EGF, respectively.

At c_{EGF} = 2 ng ml^{-1}, individual cell morphological characteristics (figure 2a) indicated that the cell spreading area was smaller than in the absence of EGF. Concomitantly, the cell-cell contact area diminished, and a large number of cells exhibited long filopodia connections. Furthermore, in these cases, cell immunostaining of vinculin protein provided information about both focal contacts between cells and the substrate. As c_{EGF} increased, the number of focal contacts increased although their average size diminished (figure 2b); these features were similar for c_{EGF} = 10 ng ml^{-1}, tending to reach a saturation effect for higher c_{EGF}. The distribution of focal contacts also depended on c_{EGF}. For cells in the control medium, focal contact distribution was rather homogeneous in the cell cytoplasm surrounding the nucleus. In contrast, in the presence of EGF, a large number of cells exhibited an increased focal contact density asymmetrically distributed. This fact was accompanied by the cytoplasm asymmetric spreading, as was more clearly appreciated by actin staining (figure 2a).

Tumor cell colonies in EGF supplemented medium

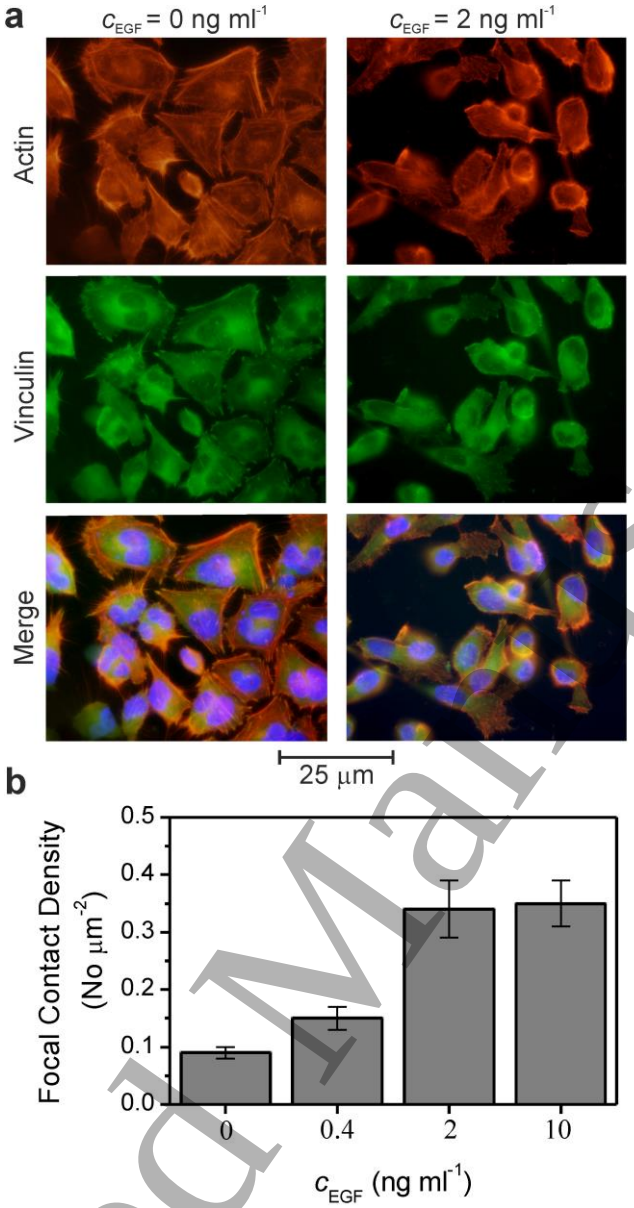

Figure 2. (a) Actin and vinculin immunostaining and merge with DAPI nucleus staining for cells seeded from control culture medium and c_{EGF} = 2 ng ml^{-1}. (b) Histogram of the number of focal contacts in cytoplasms per μm^2 for cells seeded from control medium c_{EGF} = 0 ng ml^{-1}, c_{EGF} = 0.4 ng ml^{-1}, c_{EGF} = 2 ng ml^{-1}, and c_{EGF} = 10 ng ml^{-1}

3.1.2. Kinetic data. HeLa QRCs with a value of N_0 yielding confluent colonies along the entire follow-up for all c_{EGF} allowed us to compare the kinetic behavior of colonies in the control and EGF-containing media. In these cases, the initial colony radius (R_0) in the 200 – 600 μm range was measured. The evolution of <*R*> depicted as *log* <*R*> versus *t* plots offers the possibility of a better distinction of changes in the kinetic behavior of the systems (figure 3).

Tumor cell colonies in EGF supplemented medium

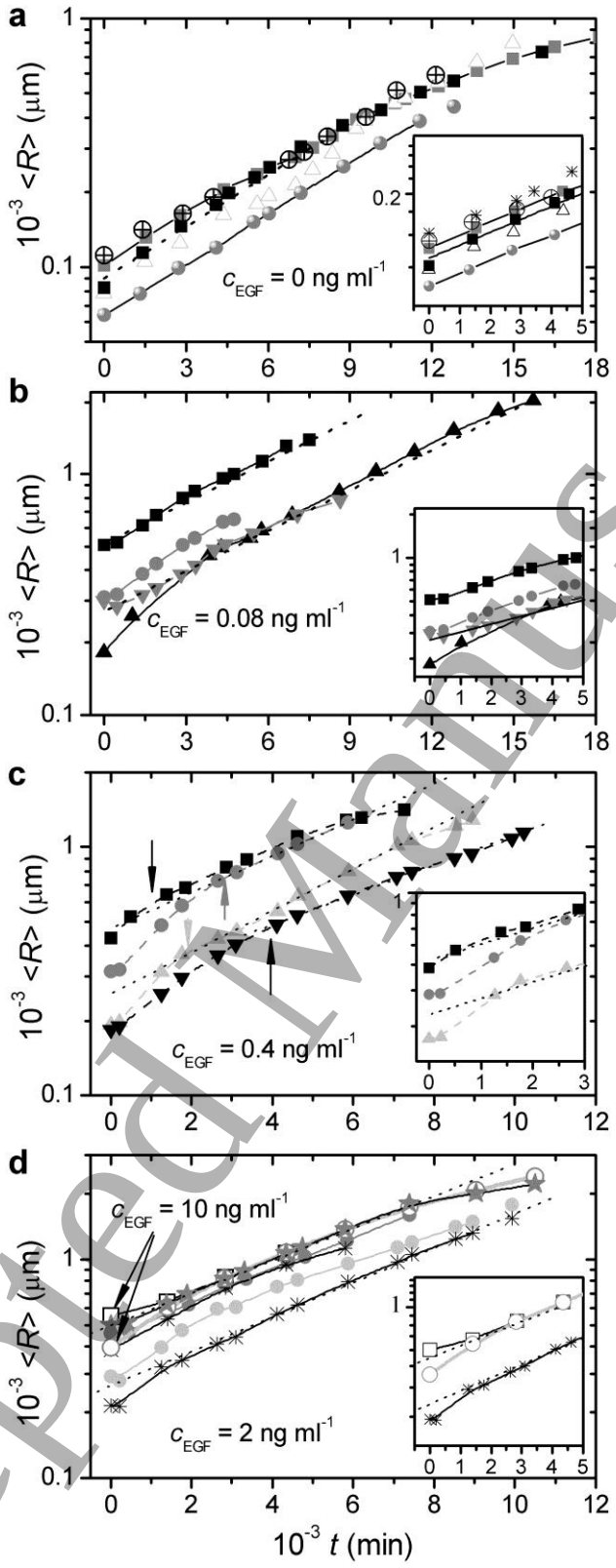

Figure 3. Semi-log <*R*> versus *t* plots from HeLa QRCs grown in media with different c_{EGF} as indicated in the figure. Lines to guide the eyes are depicted in dashed traces. Insets in the figure show the departure from the linear relationship at short *t*. Arrows in (c) indicate the transition time from the supra-exponential to the exponential growth regime.

Cell colonies in the control medium, c_{EGF} = 0 ng ml^{-1}, followed up for about 10 days, showed an average colony radius displacement <*R*> versus *t* that follows an exponential law in the range from t_0 up to t_c, but for $t > t_c$ and <*R*> > <R_c>, a constant front displacement velocity (V_F) regime was attained, in agreement with the departure from the log <*R*> versus *t* linear relationship (figure 3). From the exponential V_F dependence, the average velocity constant k = 4.2 10^{-4} min^{-1} was obtained [33]. In the presence of EGF, the dependence of the colony radius on *t* becomes more complicated than that observed for the control medium. In general, the colony front displacement velocity increases with c_{EGF}, but exhibits a relationship that depends also on the colony history. Values of <R_0>, N_0 and the initial cell density are larger for colonies growing in EGF containing media in order to obtain confluent colonies over the entire growth time range.

As depicted in figure 3b, <*R*> versus *t* plots for the lowest c_{EGF} showed only minor differences in comparison with the control medium. The colony growth kinetics exhibited the exponential regime followed by the constant velocity one, as referred to above. For relatively small <R_0> and initial densities, i.e., 0.0011 and 0.00071 cell μm^{-2}, at the initial stages of growth <*R*> showed a supra-exponential dependence on *t*. Thus, V_F increased faster than what should be expected from the exponential <*R*> versus *t* relationship.

For colonies with comparable values of N_0 and cell density and with either c_{EGF} = 0.4 or 2 ng ml^{-1} (figures 3c and d), the supra-exponential regime occurred for 0 < *t* < 4000 min, with an average colony radius versus *t* slope larger than that predicted by the exponential relationship. This trend also emerged for colonies growing in 10 ng ml^{-1} (figure 3d). Accordingly, for c_{EGF} = 10 ng ml^{-1} and colonies starting from R_0 ~ 500 μm (N_0 ≈ 1400 cells), the supra-exponential kinetic regime followed by the exponential one remains up to about 9000 min. Later, the constant velocity regime is approached. For <R_0> < 500 μm and c_{EGF} = 10 ng ml^{-1}, the constant velocity regime is absent, and the exponential colony growth extends over the full observation time.

The departure of *log* <*R*> versus *t* from the exponential colony growth kinetics at the initial stages of growth in the presence of EGF can be correlated with the colony morphology, i.e., the local change in cell density. Figure 4 shows typical <*R*> versus *t* plots and their cell colony growth pattern evolution. In the presence of EGF, either for c_{EGF} = 0.4 ng ml^{-1} or c_{EGF} = 10 ng ml^{-1}, at the first stages of growth, the supra-

exponential regime can be distinguished. This effect becomes clearer for runs with c_{EGF} = 0.4 ng ml^{-1} than for c_{EGF} =10 ng ml^{-1}. However, the larger c_{EGF} the greater the colony radius required to attain the constant velocity regime. From the colony pattern evolution, the decrease in the cell density at the colony inner regions can be observed over the time range of supra-exponential growth. In the insets of cell colony images, an increase in cell size, cell-cell separation, the presence of small voids, and a more tapered cell shape can be observed. Later, the departure from the log <*R*> versus *t* linear relationship is accompanied by a significant increase in the colony cell density. The cell colony remains confluent although cell-cell interactions are expected to change with time and at the different growth kinetic stages depending in part on the cell shape and cell-cell contact area.

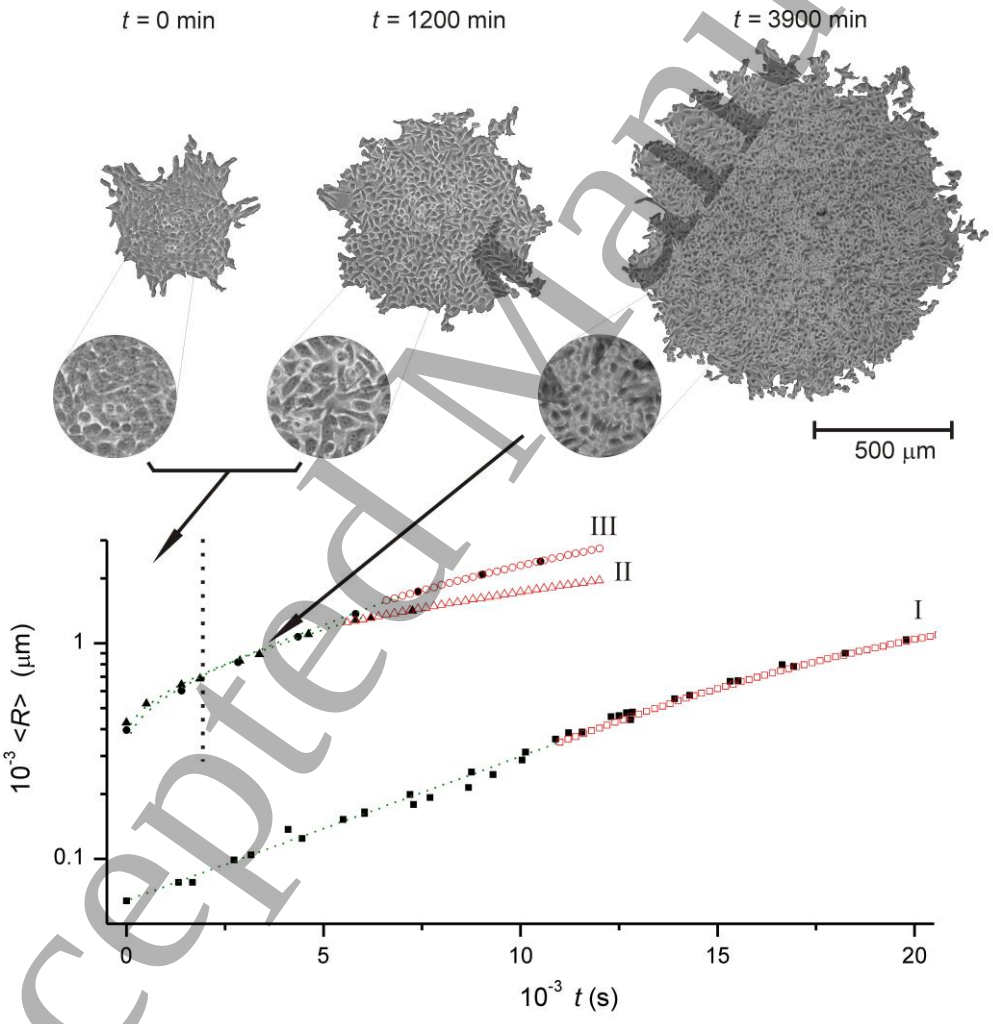

Figure 4. <*R*> versus *t* plots for c_{EGF} = 0 (I), 0.4 (II), and 10 ng ml^{-1} (III). In this case, each plot depicted in green and red discontinued traces corresponds to the adapted equations proposed by Drasdo et al. [44] (details are included in the text). The cell colony pattern for c_{EGF} = 0.4 ng ml^{-1} related to each distinctive growth kinetic regime is also included. Changes in cell morphology and density can be appreciated from the augmented insets.

Colony growth kinetic data, at the first stages of growth, fit a $Bt^{1/2} + A´\exp(Ct)$ equation (with B, A´ and C, constants that depend on the experimental conditions), and at longer time they fit an equation that describes the transition from the exponential to the constant velocity growth regime as has been proposed by Drasdo et al. [44] (color traces in figure 4). The proposed equation for the initial stages of the colony growth contains two time-dependent terms, one related to cell motion and the other to cell proliferation. Diffusion is characterized by the $t^{1/2}$ dependence, and has been proposed for modeling cell colony growth at short times [28, 45]. This matter is further reconsidered in the Discussion Section.

Summing up, the complex kinetics of the cell colony growth depends on the value of c_{EGF}, the initial colony radius and cell density, as well as on the evolution of the cell density distribution in the colony. The cell colony growth is accompanied by the development of spatiotemporal heterogeneity cell distribution at the colony. Table S1 of the Supplementary data depicts N_0, $<R_0>$, the initial density and the prevailing growth kinetic regime at different c_{EGF}. For colonies with both high N_0 and high initial cell colony density, the transition from exponential to constant velocity growth becomes more favorable. The time range of the exponential colony growth increases with c_{EGF}. The presence of EGF modifies the overall kinetics by changing the cell shape and size cell-cell separation and increasing both the cell motility and duplication rate. Concomitantly with these effects, changes in both cell-cell and cell-substrate interactions are observed. These biochemical features depend on the initial cell colony population and density, and at least in part, they appear to be also reflected in the QRC growth kinetics, as at earlier stages of growth these colonies eventually exhibited a supra-exponential growth regime together with an increase in the cell colony front velocity and changes in t_c and N_c in the presence of EGF.

For runs made with 0.4 and 2 ng ml^{-1}, the cell density profile evolution (figure 5) depends on N_0 and the initial cell density, which is consistent with the preceding kinetic description. Thus, at the first stages of growth, QRCs with a low N_0 and a high initial cell density showed a rather abrupt decrease in cell density followed by its steady increase for $t \approx 5000$ min, up to density values close to or larger than that observed at t_0. The above decrease in cell density profile is consistent with the departure from the $<R>$ versus t exponential relationship observed at the initial stages of growth. At the initial stages of growth, for QRCs growing in culture medium with c_{EGF} = 0.4 ng ml^{-1}, a large

N_0 and a small initial cell density, no cell density decrease at the initial stages of growth could be clearly distinguished. Correspondingly, the <*R*> versus *t* plot exhibited a constant colony front displacement velocity over the entire growth time range. For c_{EGF} = 2 ng ml^{-1} the decrease in the initial cell density is reflected in the appearance of the supra-exponential growth regime; the greater the initial density the more distinguishable the supra-exponential regime (figure 5). *N* versus *t* plots are included in Fig. 5 for the same experiments described above, exhibiting only a quasi-exponential behavior without the supra-exponential regime observed from <*R*> versus *t* data.

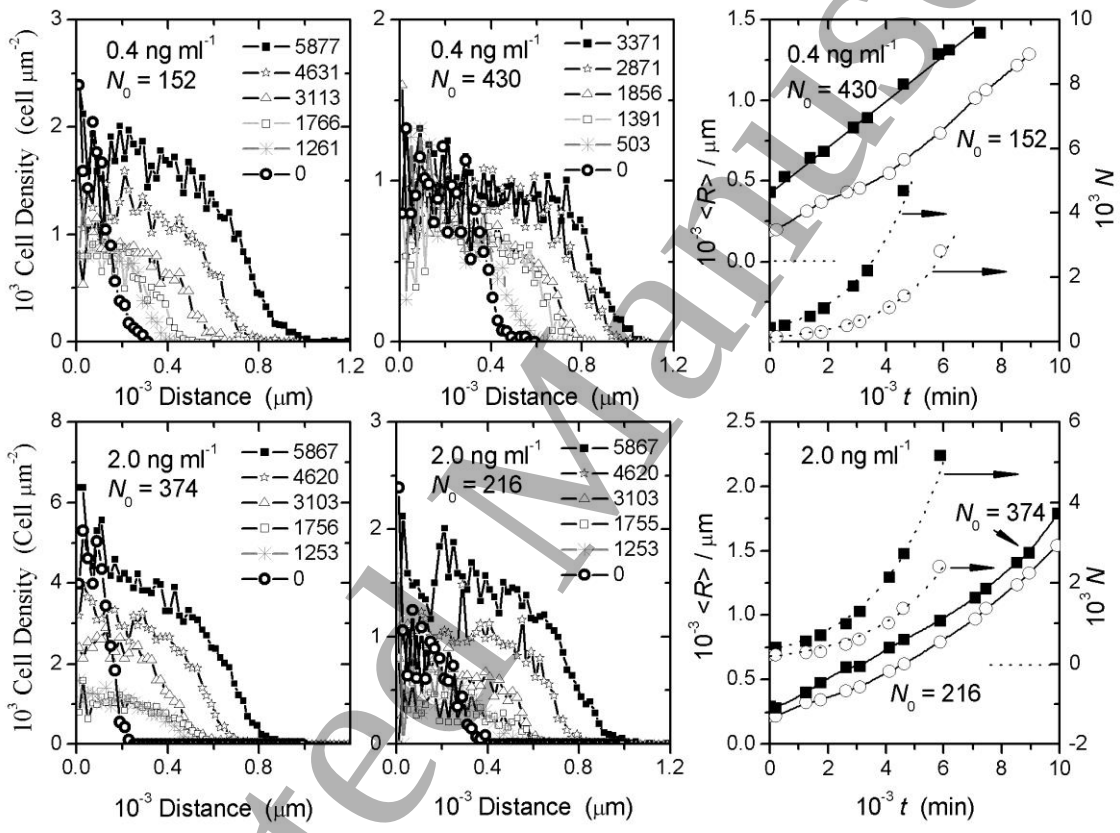

Figure 5. Density profiles and <*R*> versus *t* plots from HeLa cell colonies with different initial cell populations and cell density growing in culture media with different c_{EGF} as indicated. Those colonies exhibiting a decrease in the cell density at the first stages of growth either for c_{EGF} = 0.4 ng ml^{-1} or c_{EGF} = 2 ng ml^{-1} show a supra-exponential relationship in the <*R*> versus *t* plots for *t* up to 4000 min. *N* versus *t* data are also depicted for each experimental condition. The initial cell number for each colony, N_0, is indicated in the plots.

Otherwise, for QRCs growing in $0 \leq c_{EGF} < 0.08$ ng ml^{-1} and $c_{EGF} \geq 10$ ng ml^{-1}, a single exponential growth was found when the cell density at colony border regions increased monotonously with time. However, the greater c_{EGF} the smaller the cell density at the

colony border regions. For colonies exhibiting a time-dependent cell density gradient, their kinetic data fitted the exponential law. Conversely, as has been previously reported [33] for colonies growing at constant V_F, the cell density gradient remained unchanged for about 1000 min.

It is worth noting that density profiles can only be evaluated from those colonies in which the cell number counting is reliable. Unfortunately, for colonies with the largest N_0, and $t >> t_0$, the appearance of 3D cell domains in the colony bulk and enlarged cells at the colony border turned individual cell counting and cell density determination rather uncertain.

3.2. Quasi-linear colonies

QLCs exhibit large cell populations and constant front length that imply a constant free space contribution assisting colony propagation. These runs allowed us to determine cell motility parameters by both manual cell tracking and particle image velocimetry (PIV) [42, 46]. These data help to understand further details of the influence of the spatiotemporal colony heterogeneities on both the local cell morphology and the colony front spreading dynamics.

3.2.1. Morphology. The influence of c_{EGF} on the collective phenomena involved in the morphology evolution of QLCs is depicted in figure 6. The effect of c_{EGF} on cell morphology at QLC outer regions is to some extent comparable to that described for confluent small QRCs.

In the absence of EGF, colony pattern microimages taken 24 h after the Teflon removal revealed a gradual local cell density decrease in going from the innermost colony regions outwards. Many cells exhibited an extended cytoplasm polarized in the colony front propagation direction. Also, groups of cells at the bulk oriented towards the colony front can be observed. This morphological feature, which is also applicable at longer t (60 h), is also accompanied by a further cell density increase at inner colony regions, yielding the incipient formation of 3D clusters there and a further increase in the average cell size at the colony border. Likewise, it appears that the presence of oriented cell domains is associated with the formation of protrusions at the colony front (Figures 6a and 6b).

Tumor cell colonies in EGF supplemented medium

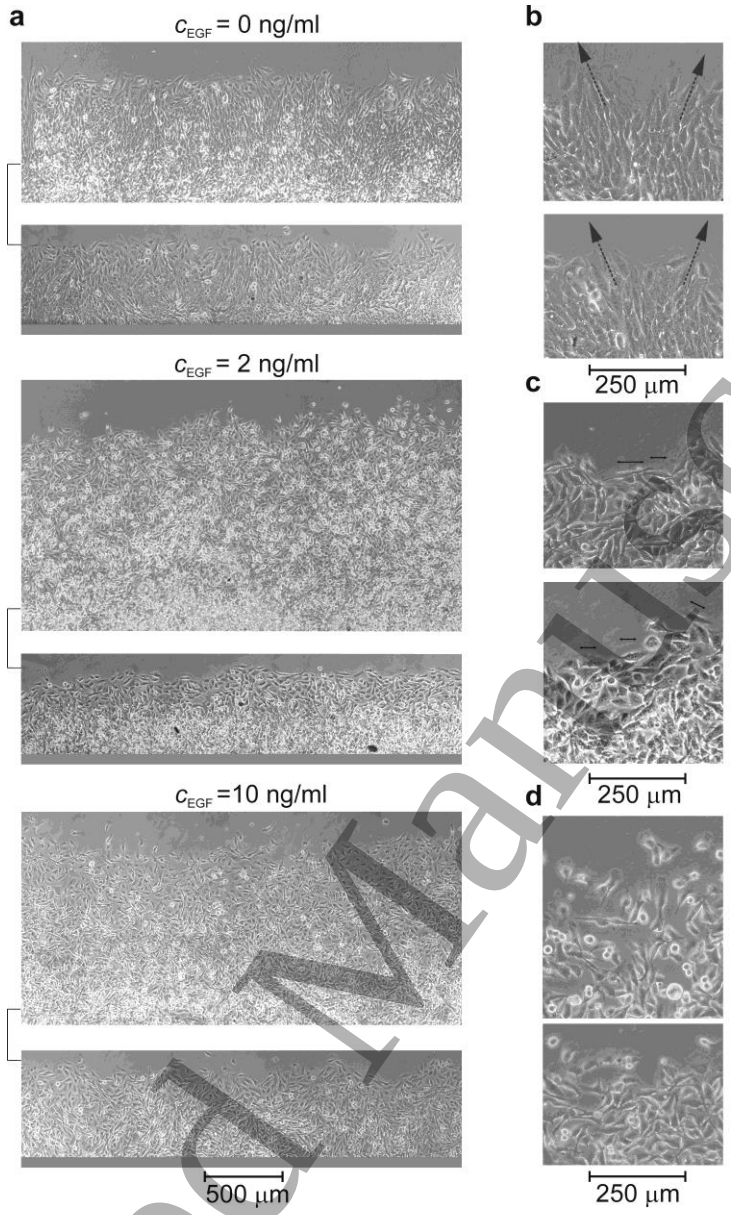

Figure 6. QLC patterns. (a) Sequences for cell cultures in media with different c_{EGF} as indicated in the figure. Images were taken at t = 24 and t = 60 h after the Teflon removal. (b) Enlarged images of cells protruding the contour of a colony growing in the culture medium with c_{EGF} = 0; the time between images is 8 h. (c) Images of a colony border sector in the culture medium with c_{EGF} = 2 ng ml^{-1}; a large number of cells are oriented parallel to the colony border (indicated in the figure by black segments). The time between images is 8 h. (d) Images of a sector of the colony border region. The colony grows in the culture medium with c_{EGF} = 10 ng ml^{-1}; the detachment of both isolated cells and groups of cells from the colony can be appreciated.

Sequences of colony patterns propagating in EGF-containing media, either with c_{EGF} = 2 or 10 ng ml^{-1} at t = 24 h and t = 60 h, are also depicted in figure 6. For t = 24 h, the colony bulk regions exhibit a higher cell density than at the colony border, as in the case of cultures in the control medium. In contrast, in the presence of EGF, the cell average

size and the extent and number of colony domains with polarized cells are significantly smaller than in the control medium. As shown in figure 6c, a large number of cells are oriented parallel to the colony front, whereas other ones in the colony bulk exhibit long filopodia connecting distant neighbor cells. These distinct behaviors are even more remarkable for t = 60 h. Otherwise, growth patterns at longer t also involve a large number of rounded cells, either under duplication or partially detached forming small cell agglomerates. It appears that the presence of EGF induces the enlargement of the 2D low density region particularly near the colony border. But, for c_{EGF} = 10 ng ml^{-1} most cells are interconnected through long filopodia. Besides, either individual cells or small groups of cells tend to detach from the colony, generating a less confluent colony border (figures 6a and 6d).

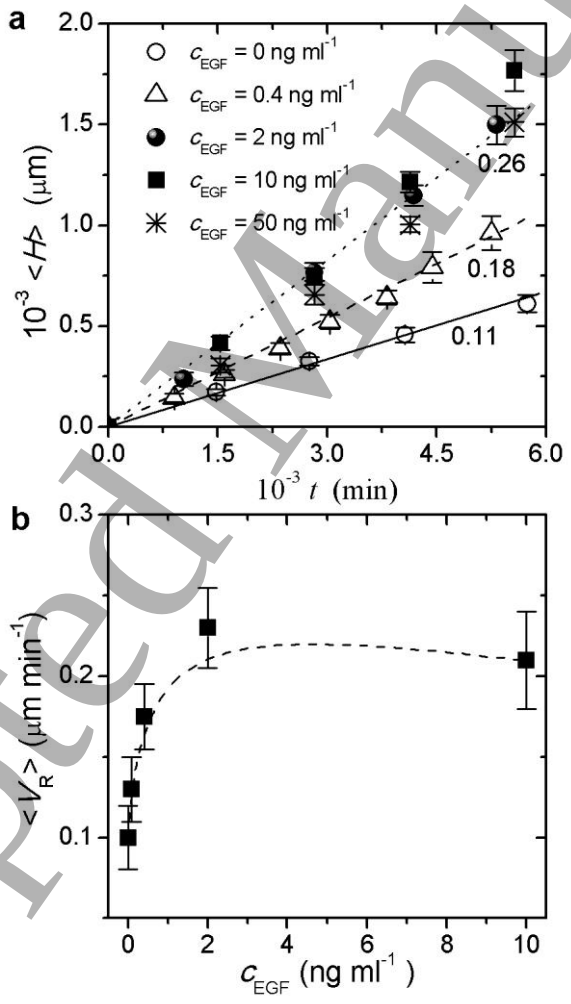

Figure 7. (a) Average QLC front displacement distances versus t plots. Data from colonies in culture media containing different c_{EGF}. The slopes (μm min^{-1}) of the plotted lines are included. (b) Average colony front displacement velocity of QRC colonies for different c_{EGF} as indicated. Standard errors are included.

3.2.2. Colony propagation kinetics. The average QLC front displacement operates at constant V_F regardless of c_{EGF}, although its magnitude increases from $\langle V_F \rangle$ = 0.11 μm min^{-1} at c_{EGF} = 0 ng ml^{-1} and c_{EGF} = 0.08 ng ml^{-1} to $\langle V_F \rangle$ = 0.18 μm min^{-1} at c_{EGF} = 0.4 ng ml^{-1}, and to $\langle V_F \rangle$ ~ 0.26 μm min^{-1} at c_{EGF} 2, 10 or 50 ng ml^{-1} (figure 7a). At the highest c_{EGF}, the colony front became rougher and exhibited a large number of disaggregated cells, making it rather uncertain for tracing the colony front contour.

The limiting average colony front displacement velocity of QRC colonies $\langle V_R \rangle$, obtained from the slope of $\langle R \rangle$ versus t plots at the linear constant velocity regime, is plotted in figure 7b. Despite the large error, mainly due to the poor definition of the constant velocity regime, a first rather abrupt increase in $\langle V_R \rangle$ with c_{EGF} and a tendency to attain saturation for c_{EGF} > 2 ng ml^{-1} is observed. Moreover, for each c_{EGF}, $\langle V_R \rangle$ values are similar to the QLC front displacement velocity, as it has been previously reported for c_{EGF} = 0 ng ml^{-1} [33].

3.2.3. Cell motility. Individual cell trajectories were tracked from QLCs in the control and EGF-containing culture media. The tracking was done considering those cells located at the first three cell layers from the colony border.

For c_{EGF} = 0, cell trajectory tracking diagrams at inner colony regions exhibited random cell displacements, whereas at outer colony regions, cell displacements involved a greater directionality. As reported above, QLCs displayed distinguishable distributions of cell density domains and the formation of protrusions at the colony border. The cell motility position-dependent characteristics should result from the cell displacement asymmetries in the colony, mainly driven by colony cell density heterogeneities (figure 6). The increase in cell density at the colony inner regions in comparison with border regions enhances cell motility asymmetry, and cell density distribution at different regions of the colony locally affects cell displacements.

Tumor cell colonies in EGF supplemented medium

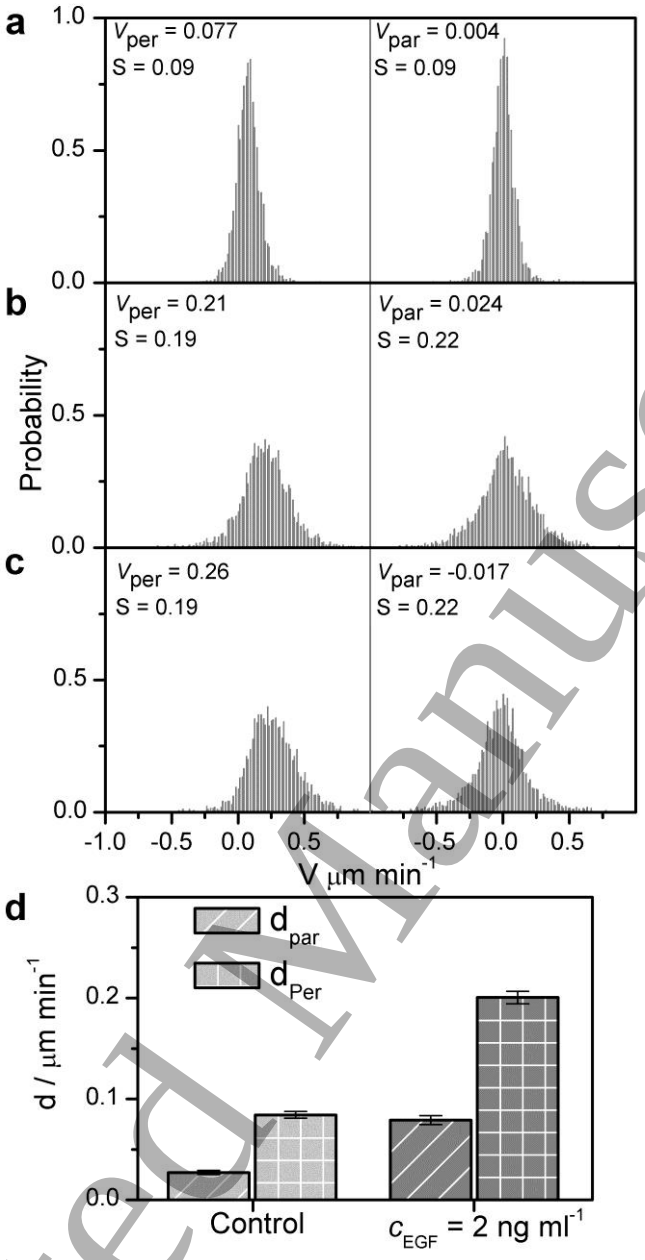

Figure 8. (a-c) Cell velocity components in control and EGF-containing media from cell trajectory tracking of cells located at the first three cell layers from the colony border: (a) c_{EGF} = 0; (b) c_{EGF} = 2 ng, cell density = 0.0012 cell μm^{-2}; (c) c_{EGF} = 2 ng, cell density = 0.00067 cell μm^{-2}. The mean values and standard deviations (S) are included. (d) Average net parallel, d_{par}, and perpendicular, d_{per}, displacements every $\Delta t'$ = 30 min. Three experiments for each condition and more than 200 cells were considered. Standard errors are included.

Tumor cell colonies in EGF supplemented medium

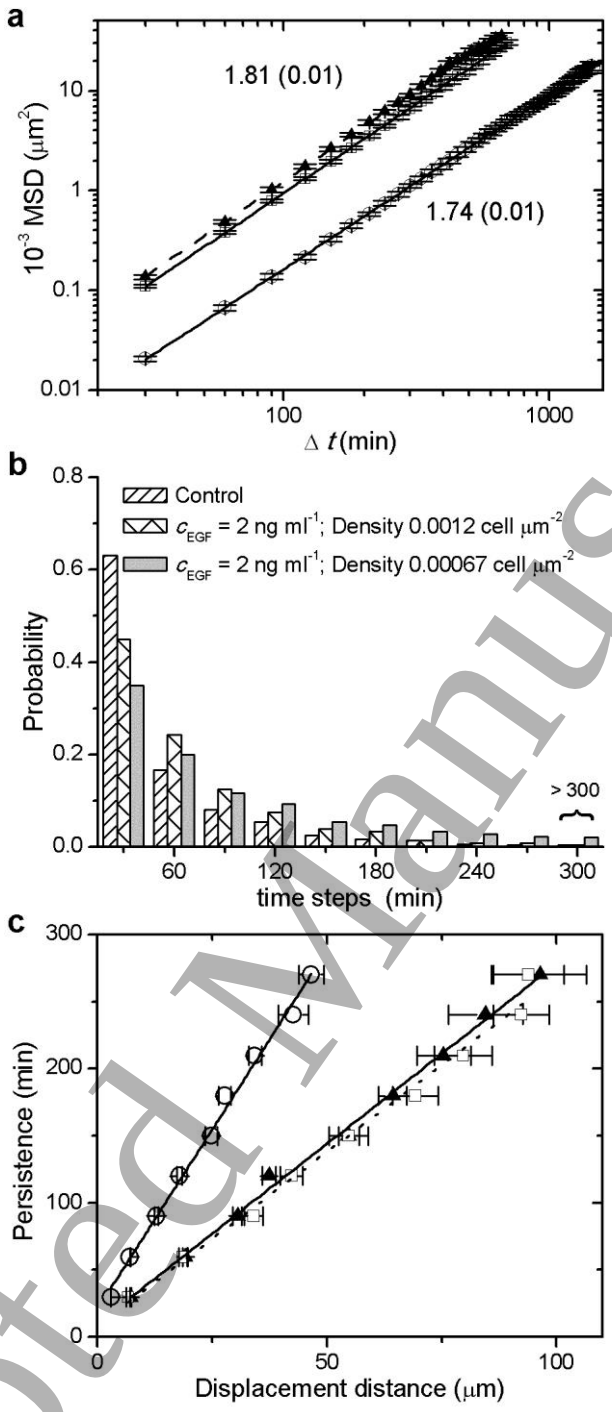

Figure 9. (a) Log-log plots of *msd* versus Δ*t* from trajectories of cells in control (○) and 2 ng ml^{-1} EGF-containing media at cell densities of 0.0012 (□) and 0.00067 cell μm^{-2} (▲). (b) Probability versus persistence plots from cell trajectories under conditions depicted in (a); the probability of observing persistent movements longer than 300 min is also included. (c) Persistence versus cell displacement distance from the same cell trajectories as in (a).

The cell trajectory tracking of colonies with c_{EGF} = 2 ng ml^{-1} and distinct initial cell densities at the border region, i.e., values close to 0.0012 and 0.00067 cell μm^{-2}, was

analyzed and compared with individual cell trajectories in the control medium. Histograms of cell velocity components parallel V_{par} and perpendicular V_{per} to the colony front are depicted in figure 8a-c. For colonies with initial cell densities close to 0.0012 cells μm^{-2}, the value of $<V_{per}>$ increased from 0.077 $\mu m\ min^{-1}$ in the control medium to 0.21 $\mu m\ min^{-1}$ in c_{EGF} = 2 ng ml^{-1} containing medium. Moreover, for a cell density of 0.00067 cells μm^{-2} and c_{EGF} = 2 ng ml^{-1}, $<V_{per}>$ further increased to 0.26 $\mu m\ min^{-1}$. On the other hand, irrespective of the experimental conditions, the value of $<V_{par}>$ was close to zero. The standard deviation (S) of both V_{per} and V_{par} increased about twice in the presence of EGF as compared to the control medium.

The presence of EGF also changed the average net parallel (d_{par}) and perpendicular (d_{per}) displacements of individual cells every 30 min (figure 8d). For c_{EGF} = 2 ng ml^{-1} and initial average cell density of 0.0012 cell μm^{-2}, d_{par} = (2.37 ± 0.12) μm and d_{per} = (6.03 ± 0.18) μm. These figures are larger than those obtained from cells in colonies growing in the control medium, i.e., d_{par} = (0.81 ± 0.06) μm and d_{per} = (2.52 ± 0.09) μm. Moreover, the quotient d_{par} / d_{per} became larger in the presence of EGF than in the control medium, being 0.39 ± 0.03 and 0.31 ± 0.02, respectively. Furthermore, the average height of protrusions was smaller in the presence of EGF in comparison to that in the absence of EGF, thus the contribution of parallel displacements should be larger in the former case.

Average log *msd* versus log Δt plots obtained from cell trajectories in colonies propagating in both the control and c_{EGF} = 2 ng ml^{-1} containing media exhibited a linear relationship, irrespective of the culture media and cell density at the colony border (figure 9a). The slopes of these plots resulted in 1.74 ± 0.04 and 1.81 ± 0.01 for the control and the EGF-containing medium, respectively. These figures show a small difference in cell motility at the colony border region with a cell density of 0.0012 and 0.00067 cell μm^{-2}. Thus, in EGF-containing medium the *msd* value is higher than in the control medium, a fact that is consistent with a greater average cell velocity at the colony border. Accordingly, for Δt = 30 min, the average cell velocity is close to 0.3 $\mu m\ min^{-1}$.

The probability of a 45 degree change in the cell displacement direction is plotted versus the time step (figure 9b). In colonies growing in 2 ng ml^{-1} EGF-containing medium, and with cell densities of 0.0012 and 0.00067 cell μm^{-2}, the 30 min cell persistence has a probability of 0.45 and 0.35, respectively. In contrast, for cells in the

control medium, the same persistence exhibits a probability close to 0.63. This probability, however, decreases faster in the control medium than in the EGF-containing one. In the former case, the above probability approached zero at about 210 min, whereas at the low cell density colony with EGF-containing medium it remained close to 0.05. Therefore, the largest persistence resulted from low cell density colonies growing in the presence of EGF. The persistence versus the average cell displacement distance plot (figure 9c) revealed that in EGF-containing medium, both the cell displacement distance and the persistence become greater than in the control medium. Consequently, those cells that move longer distances for a certain time are also the more persistent ones.

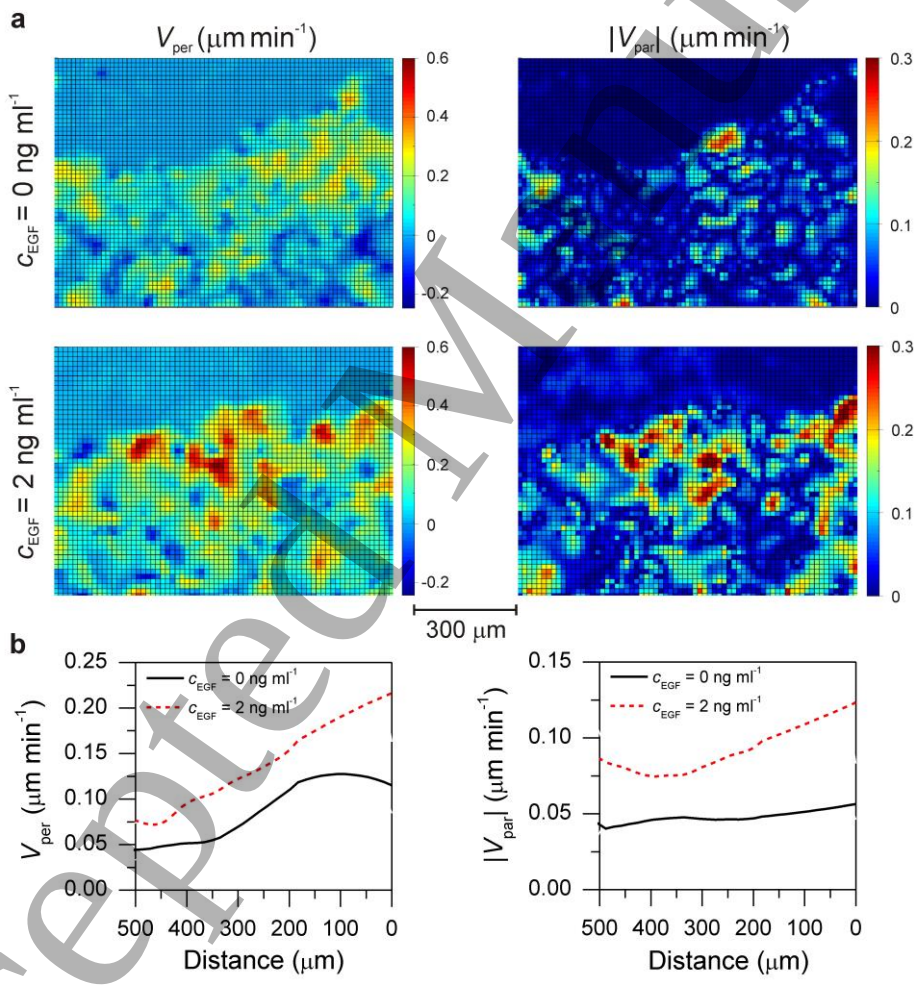

Figure 10. (a) Velocity field images for HeLa QLCs growing in the control medium and 2 ng ml^{-1} EGF-containing medium as indicated. The values of V_{per} and $|V_{par}|$ are indicated in color scale. (b) Average V_{per} and $|V_{par}|$ versus distance to the colony border plots, calculated from (a).

PIV data also indicate that cell velocity as well as the extension of the outer colony rim with highly motile cells increased in the presence of EGF (figure 10) as indicated by the color scale. The velocity components show longer vectors in 2 ng ml^{-1} EGF culture medium than for $c_{EGF} = 0$. These data are consistent with the greater extension of the effective colony rim in the presence of EGF, used in the kinetic equation proposed [44]. The analysis of the field velocity components indicates that for c_{EGF} = 2 ng ml^{-1}, it appears that the increase in the magnitude of the parallel component is larger than that observed for the perpendicular component (figure 10). This fact is in agreement with individual cell trajectory data (figure 8d). Furthermore, a trend to a faster increase of the parallel component than the perpendicular component in going from the bulk to the colony border is observed from colonies growing in EGF-containing medium (figure 10b).

3.2.4. Roughness fluctuation. According to the dynamic scaling theory [26], the interfacial roughness of a growing front of size L, $w(L,t)$, is expected to increase for $t << t_s$, where t_s is the roughness saturation time

$$w \propto t^{\beta} \quad t << t_s \tag{5}$$

and when $t > t_s$, roughness saturation w_s is attained. Then, w_s should increase with L according to

$$w_s \propto L^{\alpha} \quad t >> t_s \tag{6}$$

Moreover, the value of t_s depends on the system size

$$t_s \propto L^{Z} \quad z = \alpha / \beta \tag{7}$$

$z = \alpha/\beta$ being the dynamic exponent.

Accordingly, for a set of scaling exponents one expects the fulfillment of the Family-Vicsek relation

$$\frac{w(L,t)}{L^{\alpha}} \propto f\left(\frac{t}{L^{Z}}\right) \tag{8}$$

On the other hand, a more generic scaling analysis considers the structure factor $S(k^{c}t)$ of the entire ($s\psi = L$) growth front [26, 47, 48]

$$S(k,t) = k^{-(2\alpha_S+1)} f\left(kt^{1/Z}\right) \tag{9}$$

where α_s is the spectral roughness exponent and $f\psi(x = \quad kt^{1)z})$ the scaling function that depends on $x\psi$as follows

$$f(x) = \begin{cases} \text{const} & \text{for } x >> 1 \\ x^{(2\alpha_S+1)} & \text{for } x << 1 \end{cases} \qquad \textbf{(10)}$$

The advantage of estimating the scaling exponents in the Fourier space instead of over real space methods is that in the former case only long wavelength modes contribute to the front scaling. Real space scaling [Eq. (8)] involves all wavelength modes, including short ones, so that stronger finite size effects should be expected.

In the presence of EGF, within a range of *t* and *l* that differs from that of colonies growing in the control medium [30], the KPZ equation provides a reasonable description of the colony front dynamics (figure 11). Hence, values of α from *w* versus *L*, as well as α_S from the Fourier analysis, confirm that colony front roughness fluctuations fulfill, at least for certain range of *l* and *t*, the standard KPZ equation (figure 11).

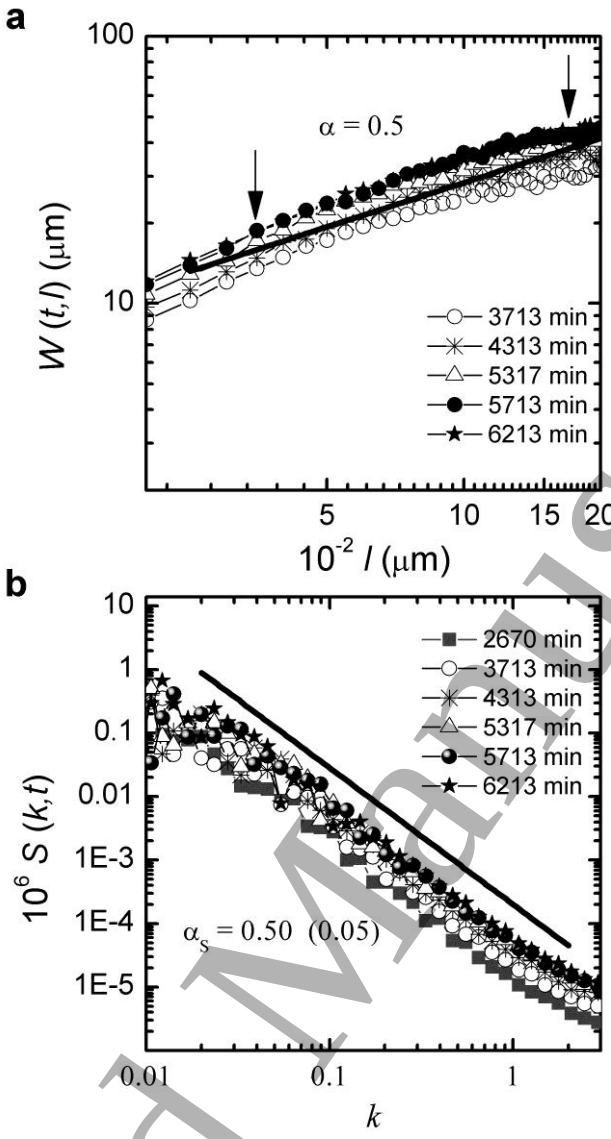

Figure 11. $W(l, t)$ versus log l (a) and S(k, t) versus k (b) log-log plots from colonies with c_{EGF} = 2 ng ml^{-1}.

Otherwise, $w(l,t)$ versus t plots from different front sizes, l, are depicted in figure 12. In the control medium, the colony front exhibits roughness saturation in the range $200 \leq l \leq 1200$ μm; for $l > 1200$ μm a linear log-log relationship with a slope β close to 0.34 results, as predicted by the KPZ equation. The presence of EGF in the medium increases the roughness of the colony front, at both the colony and the cellular scales. Data from colonies propagating in c_{EGF} = 2 ng ml^{-1} culture medium indicate that the front roughness increases continuously without saturation for l up to 900 μm, but saturation occurs at larger l values. Surprisingly, for c_{EGF} = 10 ng ml^{-1} in the culture medium, the roughness saturation is better observed only at intermediate values of l.

Tumor cell colonies in EGF supplemented medium

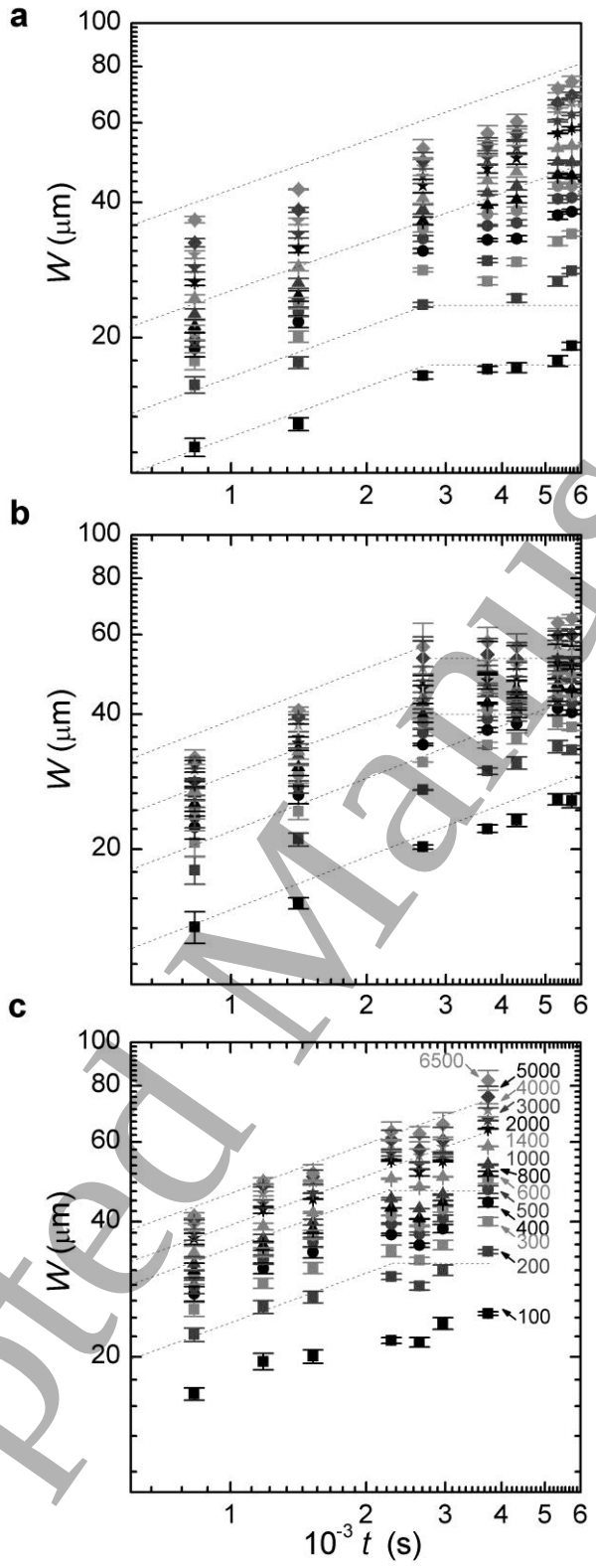

Figure 12. $W(l, t)$ versus t log-log plots for different l. Binned data from five QLCs propagating in different media. (a) Control medium, (b) with c_{EGF} = 2 ng ml^{-1}, and (c) with c_{EGF} =10 ng ml^{-1}. Roughness was analyzed for values of l indicated in (c). Standard error bars are indicated.

4. **Discussion**

4.1. Kinetics and cell morphology aspects of QRCs and QLCs in EGF-containing medium

HeLa cells are sensitive to the presence of EGF, since after binding with a cell surface receptor it activates different signaling pathways [49]. Therefore, both individual cell and the whole colony morphology depend on c_{EGF} (figures 1 and 2). The presence of EGF decreased the size of focal contacts, although their number per cell increased, attaining a saturation effect as concluded from figure 2. This is a relevant fact that agrees with fast kinetics for the adhesion/detachment process [50, 51]. Likewise, those changes in cytoskeletal organization and focal contact characteristics correlate with cell motility behavior [52].

Data have shown that QRCs exhibit a c_{EGF} dependent morphology evolution and propagation kinetics (figures 3 and 4). The effect of c_{EGF} on these processes depends mainly on N_0 and the local cell density. In general, for relatively large N_0 and colony cell densities, a linear increase in the average colony radius prevails, whereas for both relatively small N_0 and colony cell densities, the supra-exponential behavior at the initial kinetic stages of growth, followed by the exponential regime, is observed. Cell density evolution and the N versus t exponential relationship for $0.4 \leq c_{EGF} \leq 2$ ng ml^{-1}(figure 7), indicate that the supra-exponential growth could be mainly due to the contribution of cell size and cell-cell distance increase, change in shape and the enhanced cell motility at the monolayer (figures 8-10), and consequently a more effective colony contour propagation (figures 3 and 4).

Proposed colony growth models [28, 44, 45] have considered that the radial cell colony propagation comprises three stages, namely, a diffusion regime that follows a $<R>$ versus $t^{1/2}$ relationship, followed by an exponential regime, and a subsequent decrease in the colony propagation velocity characterized by a linear relationship between $<R>$ and t [44]. It should be noted that in experiments with confluent colonies growing in standard culture medium, the first kinetic regime disappeared and only the exponential growth regime followed by the constant velocity regime set in [28, 45].

This behavior has been mathematically described by a two-part equation [44] where the growing colony cross-section was approached as an outer ring of effective thickness $\Delta L_{eff} = R(t) - R_2(t)$ and a central core of instantaneous radius $R_2(t)$ associated with the

delaying effect. Then, at $t = 0$, $N = N_0$, and $R = R_0 < \Delta L_{\text{eff}}$, the transition from the exponential to constant velocity regime has been successfully obtained, in agreement with experimental data [33, 41].

The colony dynamics involves a number of processes that influence the global behavior of the system. Each process contribution depends on the growing stage of the colony, and on the growing conditions, namely c_{EGF}, the colony population, the colony age, among others, and cooperates to render the global properties of the system. The proposed equation [44] is an interesting contribution that reflects the global heterogeneities developed during the colony growth. The model simplifies the description employing macroscopic variables rather than the follow-up of the evolution of each component and the medium interacting with them.

In this case, based upon the preceding results, within a certain c_{EGF} range, the fast increase in the colony radius at the first stages of growth is enhanced. Then, the $t^{1/2}$ term become relevant and can be introduced in the equation proposed in [44], taking into account the different initial conditions (N_0, colony cell density, and c_{EGF}). Then, the modified equation resulted in

$$< R >= \begin{cases} A\left(\tau^{-1} + \phi\right)t^{1/2} + A' \exp\left(\dfrac{t}{2\tau}\right) & t \le t_{\text{c}} \\ \pi^{1/2}\,\dfrac{\Delta L_{\text{eff}}}{2}\left[1 + W\left(\dfrac{A'^{2}\, r_{\text{c}}^{2}}{\pi\, \Delta L_{\text{eff}}^{4}}\right)\exp\left(1 + \dfrac{2t}{\tau}\right)\right] & t > t_{\text{c}} \end{cases} \qquad \textbf{(11)}$$

with $W(x)$ being the Lambert function, (r_{c}) the cell radius, (τ) its duplication time, (A') the initial colony radius, $B = A(\tau^{-1} + \phi)$ a fitting the parameter with A, a constant associated with the initial colony characteristics and ϕ the cell diffusivity, and t_{c} the transition time to the constant colony front velocity regime. The latter is approached as ΔL_{eff} attains a constant value. The plot of our experimental data according to Eq. 11, considering the colony growth conditions, listed in Table 1, resulted in a reasonable agreement (figure 4).

Table 1. QLC growth conditions, c_{EGF}; cell colony initial properties, N_0 and A'; cell duplication time, τ; cell average radius, r_c; fitting parameters B and ΔL_{eff} employed to describe experimental data with equation 11.

Colony growth conditions						Fitting parameters	
c_{EGF} / ng ml^{-1}	N_0	r_c / μm	Cell density / N μm^{-2}	τ / min	A' / μm	B	ΔL_{eff} / μm
0	16	16	0.00124	3250	64	0	200
0.4	430	20.8	0.00074	3200	360	0.0792	240
10	1338	10.8	0.00272	2800	317	0.10144	440

The departure from the exponential growth regime at the first stages of growth should be favored in QRCs with small N_0, but with an appropriate cell density value where the contribution of cell diffusion could be distinguished. Similarly, for sufficiently large values of N_0, the higher c_{EGF} the larger ΔL_{eff}, and consequently, the longer t_c.

The values of $\langle V_R \rangle$ from QRCs growing at the constant velocity regime for each c_{EGF} approach those obtained from QLCs with the same c_{EGF}. QLCs involve large N_0 and high density domains at inner regions, and exhibit a constant velocity growth regime, attaining a limiting value $\langle V_F \rangle = 0.26 \pm 0.05$ μm min^{-1} irrespective of c_{EGF}, from $c_{EGF} >$ 2 ng ml^{-1} (figure 7). This $\langle V_F \rangle$ value was three times larger than in the control medium. For QLCs, the ΔL_{eff} is formed almost immediately, and no transient can be distinguished.

For $c_{EGF} \geq 10$ ng ml^{-1}, the detachment of both individual cells and groups of cells from the colony (figure 6), which could be related to the loose cell-cell adhesions in the colony, is observed. Cell shape and size, and their orientation in relation to the colony contour, change dramatically in the presence of EGF. In the next section, cell motility characteristics are discussed in order to explain the contribution of the above morphological changes.

4.2. Individual cell motility behavior from QLCs

Correlations between cell motility characteristics and the global dynamics of the QRCs and QLCs were also approached considering that cell displacements can be tackled

roughly by transport equations either disregarding or taking the cell size as variable [53, 54]. Thus, it is possible to map transport equations that involve no linear diffusion contributions to general complex condensed phase growth equations [26] such as those proposed from the dynamic scaling analysis. Likewise, the processes described for QRC take place at a size scale that would affect the QLC dynamics locally. The increase in the collective behavior of HeLa cell displacement with the size of QRCs should be mainly attributed to a crowding effect [33]. The latter is enhanced in QLCs due to space restrictions [55], which only exhibit a constant V_F regime. For QRCs with large $N_0 >$ 1200 and cell density larger than 0.0026 cell μm^2, the colony propagates at constant velocity. The supra-exponential coupling to the exponential regime would be observed in colonies with a cell number and density appropriate to generate a cooperative effect on the colony propagation based on changes in cell shape and separation, duplication, and migration.

Our results show that in the presence of EGF, cell displacements are more persistent and ballistic (figure 9), as reported, for instance, for mammary epithelial cell migration [56]. Furthermore, in our case, an increase in the cell average lateral displacement with respect to the forward one (figures 8d and 10) was observed. The colony density influences the cell velocity magnitude, the larger the latter the lower the cell density (figures 8 and 9). Moreover, for intermediate values of c_{EGF} ($0.08 \leq c_{EGF} \leq 2$ ng ml^{-1}) cells appear to be connected by long filopodia and at the border region, they tend to form small groups of moving cells.

PIV data (figure 10) indicate that in the presence of EGF the cell velocity is larger than that resulting from colonies growing in the control medium, and maintains a value larger than a half of the maximum cell velocity for distances from the colony border twice the one measured for the control medium. Correspondingly, the effective rim significantly increases in the presence of EGF, in agreement with the preceding kinetic data that indicate that the extension of the outer colony rim with highly motile cells increases in the presence of EGF, and the velocity components show longer vectors in 2 - 10 ng ml^{-1} EGF culture medium than for $c_{EGF} = 0$. Moreover, PIV data show a larger contribution of lateral displacements in the presence of EGF, in consonance with individual cell trajectories, cell morphology and its relative orientation respect to the colony border (figure 6).

Colony propagation data plotted as <*R*> and <*H*> versus *t* (figure 7) exhibit a tendency to attain a limiting value for the colony propagation velocity as c_{EGF} increases. This fact indicates that the EGF-enhanced cell motility would also reach saturation. A similar behavior has been reported for MCF-7 breast cancer cells stimulated with IGF (insulin growth factor) in a migration assay [57]. In our experiments, it should be pointed out that for the largest c_{EGF} the detachment of individual cells and groups of cells would make the analysis rather unfeasible. For colonies remaining confluent, the increase in c_{EGF} in the range $0.08 < c_{EGF} < 2 - 10$ ng ml^{-1}produces an increase in cell duplication, as well as changes in cell morphology and in the number and size of focal contacts. In any case, all these changes are coupled and depend on time, i.e., the colony age, location in the colony and the developed heterogeneities.

4.3. Dynamic scaling analysis

Results from the dynamic scaling analysis of both QRC and QLC fronts in the control medium for either transformed or tumor cells revealed that, at least for certain ranges of *t* and *l*, their dynamics fulfill the Kardar-Parisi-Zhang equation [58, 30]. The scaling analysis of colony contour roughness fluctuations for different c_{EGF} allows us to envisage a colony growth dynamics compatible with the standard KPZ equation in ranges of *t* and *l* different than in the control medium (figures 11 and 12). At constant *l*, a clear roughness saturation was observed in the presence of EGF, particularly for c_{EGF} = 2 ng ml^{-1} (figure 12). It is worth noting that for QLCs in media with EGF, and for $l <$ 300 μm, contrarily to the expected behavior, roughness saturation was absent. At this length scale, the changes in cell size and morphology and the rapid membrane fluctuations produced by the EGF would interfere with the colony contour scaling properties.

These results can be associated with previously described colony characteristics. Thus, in growth media with EGF, cells become more tapered and acquire an orientation parallel to the colony front. The persistence and the ballistic characteristics of cell displacements are enhanced in polarized, fast moving cells that appear in this culture medium. Concomitantly, the colony front displacement velocity reaches a maximum value within the range $2 \leq c_{EGF} < 10$ ng ml^{-1}, and the colony border remains confluent along the follow-up for c_{EGF} up to 10 ng ml^{-1}, with a larger contribution of cell displacement parallel to the colony front in comparison with data from colonies in the

absence of EGF, promoting the earliest saturation of the roughness contour in the presence of EGF. This fact can be interpreted by the relevance of the nonlinear term in the standard KPZ equation related to the lateral growth and parallel correlation length. For $c_{EGF} \geq 10$ ng ml^{-1}, a fraction of either individual cells or groups of them are likely to detach from the colony. As shown in figure 12c, this process increases the roughness of the colony contour, and the roughness saturation is roughly observed; furthermore, for this condition the contour definition begins to fail, as has been commented for QRC and small N_0. These distinct EGF-induced cell behaviors observed for intermediate values of c_{EGF} are also consistent with the observation of cell motility reported in the literature [52, 59]. Furthermore, the results corroborate the usefulness of the proposed growth equation and settle a bridge between processes at the cellular and colony scale.

5. Conclusions

* The epidermal growth factor (EGF) affects cell-cell interactions and promotes a fast cell displacement, leading to sparse cell colonies. In the presence of EGF, to attain confluent colonies, large values of N_0 and initial cell densities are required.

* Data comparison of colonies growing in control medium with those in EGF-containing medium indicates that EGF produces morphological changes at the cell and colony levels. The presence of EGF enhances the appearance of cells with large filopodia, cell orientation in the direction parallel to the growth front, and eventually cell detachment from the colony, rendering a colony border region with a lower cell density that extends longer distances from the colony border inwards.

* Colonies growing in EGF-containing medium exhibit average radius versus t plots with a transition from exponential kinetics to a constant V_F, as in the case of colonies growing in the control medium. Furthermore, mitogenic and chemotactic properties of EGF perturbed the QRC border displacement kinetics, by increasing the front displacement velocity and the magnitude of both t_c and R_c, and producing a supra-exponential growth regime at earlier stages of growth for colonies with intermediate values of N_0 and cell densities.

* The presence of EGF increases the individual cell velocity and affects the contribution of velocity components parallel to the colony front, as well as the persistence and ballistic characteristics of cell trajectories. Moreover, as c_{EGF} is increased, cells from

deeper layers of the colony have net velocities towards the colony front and also contribute to the propagation of the colony.

* The growth kinetics of colonies in EGF-containing medium is reasonably adjusted by a mathematical model proposed in [40] including a $t^{1/2}$ term to fit the supra- exponential growth at the earlier stages of growth. Then, this model agrees with the increase in the effective rim and t_c caused by the presence of EGF in the medium.

* In comparison with colonies growing in the control medium without EGF, at intermediate values of c_{EGF}, persistent cooperative cell displacements in the border regions influence the roughening of the colony contour, which is reasonably described by the standard Kardar-Parisi-Zhang growth model with faster roughness saturation. The presented strategy is suitable to study the effects of other growth factors that modify the cellular phenotype and affect the colony evolution.

These results are of general interest for the development of feasible models to describe complex systems as well as to improve strategies and protocols in the field of wound healing and cancer research.

Acknowledgements

This work was supported by the Consejo Nacional de Investigaciones Científicas y Técnicas of Argentina, CONICET (PIP 0602), the Comisión de Investigaciones Científicas (CIC), Pcia. Bs. As., Agencia Nacional de Promoción Científica y Tecnológica (ANPCyT, Argentina; PICT-163/08, PICT-2010-2554, and PICT-2013-0905), the Austrian Institute of Technology GmbH (AIT–CONICET Partner Group: "Exploratory Research for Advanced Technologies in Supramolecular Materials Science," Exp. 4947/11, Res. No. 3911, 28-12-2011), and Universidad Nacional de La Plata (UNLP). M.A.P. and O.A. are staff members of CONICET.

References

1. A Wells 2006 *Cell Motility in Cancer Invasion and Metastasis* (The Netherland: Springer)

2. Simpson C L, Patel D M, Green K J 2011 *Nat. Rev. Mol. Cell Biol.* **12** 565

3. Behm B, Babilas P, Landthaler M, Schreml S 2012 *JEADV* **26** 812

4. Borena B M, Martens A, Broeckx S Y, Meyer E, Chiers K, Duchateau L, Spaas J H 2015 *Cell Physiol. Biochem.* **36** 1

5. Ceresa B P, Peterson J L 2014 *International review of cell and molecular biology*. Vol. 313 Chapter five – *Cell and molecular biology of epidermal growth factor receptor* ed. J Kwang (Waltham: Elsevier) p 145

6. Mitsudomi T, Yatabe Y 2010 *FEBS J.* **277** 301

7. Maheshwari G, Wells A, Griffith L G, Lauffenburger D A 1999 *Biophys. J.* **76** 2814

8. Kurten R C, Chowdhury P, Sander Jr R, Pittman L M, Sessions L W, Chambers T C, Lyle C S, Schnackenberg B J, Jones S. M. 2005 *Am. J. Physiol. Cell Physiol.* **288**, C109

9. Berkers J A, van Bergen en Henegouwen P M, Boonstra J 1991 *J. Biol. Chem.* **266** 922

10. Capuani F, Conte A, Argenzio E, Marchetti L, Priami C, Polo S, Di Fiore P P, Sigismund S, Ciliberto 2015 *Nat. Commun.* **6** 7999

11. Dürer U, Harting R, Bang S, Thim L, Hoffmann W 2007 *Cell. Physiol. Biochem.* **20** 329

12. Seeger M A, Paller A S 2015 *Advances in Wound Care* **4** 213

13. Pope M D, Graham N A, Huang B K, Asthagiri A R 2008 *Cell Adh Migr* **2** 110

14. Ware M F, Wells A, Lauffenburger D A 1998 *J. Cell Sci.* **111** 2423

15. Geum D T, Kim B J, Chang A E, Hall M S, Wu M 2016 *Eur. Phys. J. Plus* 131 **8**

16. Kim C S, Mitchell I P, Dosetell A W, Kreeger P K, Masters K S 2016 *FASEB Journal* **30** 1

17. Wickert LE, Pomerenke S, Mitchell I, Masters K S, Kreeger P K 2016 *Sci. Rep.* **6** 20139

18. Friedl P, Glimour D 2009 *Nat. Rev. Mol. Cell Biol.* **10** 445

19. Haeger A, Wolf K, Zegers M M, Friedl P 2015 *Trends Cell Biol* **25** 556

20. Rappel W J 2016 *Proc. Natl. Acad. Sci. U. S. A.* **113** 1471

21. Ellison D, Mugler A, Brennan M D, Lê S H, Huevner R J, Shamir E R, Woo L A, Kim J, Amar P, Nememan I, Ewald E J, Levchenko A 2016 *Proc. Natl. Acad. Sci. U. S. A.* **113** E679–E688.

22. Chepizhko O, Giampietro C, Mastrapasqua E, Nourazar M, Ascagni M, Sugni M, Fascio U, Leggio L, Malinverno C, Scita G, Santucci S, Alava M J, Zapperi S, La Porta C A M 2016 *Proc. Natl. Acad. Sci. U. S. A., Early ed.* **113** 11408

23. Galeano J, Buceta J, Juarez K, Pumariño B, de la Torre J, Iriondo J M 2003 *Europhys. Lett.* **63** 83

24. Bonachela J A, Nadell C D, Xavier J B, Levin S A 2011 *J. Stat. Phys.* **144** 303

25. Takeuchi K A 2014 *J. Stat. Mech* P01006

26. Barabasi A L, Stanley, H E 1993 *Fractal Concepts in Surface Growth* (Cambridge: Cambridge University Press)

27. Meakin P 1998 *Fractals, Scaling and growth far from Equilibrium* (Cambridge: Cambridge University Press)

28. Block M, Schöll E, Drasdo D 2007 *Phys. Rev. Lett.* **99** 248101

29. Huergo M A C, Pasquale M A, González P H, Bolzán A E, Arvia A J 2011 *Phys. Rev.* E **84** 021917

30. Huergo M A C, Pasquale M A, González P H, Bolzán A E, Arvia A J 2012 *Phys. Rev.* E **85** 011918

31. Moon K-W, Kim D-H, Yoo S-C, Cho C-G, Hwang S, Kahng B, Min B-C, Shin K-H, Choe S-B 2013 *Phys. Rev. E* 110 107203

32. Almeida R A L, Ferreira S O, Oliveira T J, Aarão Reis F D A 2014 *Phys. Rev. B* **89** 045309

33. Muzzio N E, Pasquale M A, González P H, Arvia A J 2014 *J. Biol. Phys*. **40** 285

34. Chen J, Zeng F, Farrester S J, Eguchi S, Zhang M-Z, Harris R C 2016 *Phys. Revs.* **96** 1025

35. Treloar K K, Simpson M J, Haridas P, Manton K J, Leavesley D, Elwain D L S M, Baker R E 2013 *BMC Systems Biology* **7** 137

36. Hou Y, Heldberg S, Schneider I C 2012 *BMC Biophysics*, **5:8**. DOI: 10.1186/2046-1682-5-8

37. Sawyer C, Sturge J, Bennett D C, O'Hare M J, Allen W E, Bain J, Jones G E Vanhaesebroeck B 2003 *Cancer Res.* **63** 1667

38. Poujade M, Grasland-Morgain E, Hertzog A, Chavrier P, Ladoux B, Buguin A, Silberzan P 2007, *Proc Natl Acad Sci U S A* **104** 15988

39. Horzum U, Ozdil B, Pesen-Okvur D 2014 *MethodsX* **1** 56

40. Diambra L, Cintra L C, Chen Q, Schubert D and Costa L da F 2006 *Physica* A **365** 481 90

41. Li L, Wang B H, Moalim-Nour S, Mohib K, Lohnes D and Wang L 2010 *Biophys. J.* **98** 2442

42. Petitjean L, Reffay M, Grasland-Mongrain E, Poujade M, Ladoux B, Buguin A, Silberzan P 2010 *Biophys. J* 88 1790

43. Thielicke W, Stamhuis E. 2014 *Journal of Open Research Software* **2** e30

44. Radszuweit M, Block M, Hengstler J G, Schöll E, Drasdo D 2009 *Phys. Rev.* E **79** 051907

45. Drasdo D 2005 *Advances in Complex System* **8** 319

46. Muzzio N E, Pasquale M A, Huergo M A C, Bolzán A E, González P H, Arvia A J 2016 *J. Biol. Phys*. **42** 477

47. Ramasco J, López J M, Rodríguez M A 2000 *Phys. Rev. Lett.* **84** 2199

48. López J M, Rodríguez M A, Cuerno R 1997 *Phys. Rev.* E **56** 3993

49. Oda K, Matsuoka Y, Funahashi A, Kitano H 2005 *Mol. Syst. Biol*. **1** 1

50. Xie H, Pallero M A, Gupta K, Chang P J, Ware M F, Witke W, Kwiatkowski D J, Lauffenburger D A, Murphy-Ullrich J E, Wells A 1998 *Cell Sci.* **111** 615

51. Rijken P J, Hage W J, Henegouen P M P V E, Verkleij A J, Boonstra J 1991 *J. Cell Sci.* **100** 491

52. Hou Y, Hedberg S, Schneider I C 2012 *BMC Biophys*. **5** 8

53. Deroulers C, Aubert M, Badoual M, Grammaticos B 2009 *Phys. Rev.* E **79** 031917–13

54. Simpson M J, Baker R E, McCue, S W 2011 *Phys. Rev.* E **83** 021901–14

55. Marel A-K, Zorn M, Klingner C, Wedlich-Söldner R, Frey E, Rädler J O 2014 *Biophys. J.* **107** 1054

56. Maheshwari G, Wiley H S, Lauffenburger D A 2001 *J. Cell. Biol*. **155** 1123

57. Simpson M J, Chris Towne, Sean MacElwain D L, Upton Z 2010 *Phys. Rev. E.* **82**, 041901

58. Kardar M, Parisi G, Zhang Y-C 1986 *Phys. Rev. Lett.* **56**, 889

59. Harms B D, Bassi G M, Horwitz A L, Lauffenburger D A 2005 *Biophys. J.* ***88*** 1479